Nonequilibrium condensation and coarsening of field-driven dipolar colloids

Sebastian Jäger,* Heiko Schmidle, and Sabine H. L. Klapp
Institute of Theoretical Physics, Technical University Berlin, Hardenbergstraße 36, 10623 Berlin, Germany
(Received 7 May 2012; published 9 July 2012)

In colloidal suspensions, self-organization processes can be easily fueled by external fields. Here we consider monolayers of particles with permanent dipole moments that are driven by rotating external fields. In recent experiments, it has been shown that the particles in such systems self-organize into two-dimensional clusters. Here we report results from a computer simulation study of these pattern forming systems. Specifically, we employ Langevin dynamics simulations, Brownian dynamics simulations that include hydrodynamic interactions, and Wang-Landau Monte Carlo simulations of soft spheres interacting via dipolar potentials. We investigate at which field strengths and frequencies clusters form and explore the influence of hydrodynamic interactions. We also examine the phase behavior of the equilibrium system resulting from a time average of the colloidal interactions in the rotating field. In this way we demonstrate that the clustering described in the driven system arises from a first-order phase transition between a vapor and a condensed phase.

DOI: 10.1103/PhysRevE.86.011402 PACS number(s): 82.70.Dd, 81.16.Dn, 75.75.Jn

I. INTRODUCTION

Self-assembly and self-organization processes of colloidal particles are topics that have recently been receiving much attention. Indeed, such systems display a multitude of equilibrium and nonequilibrium self-assembled structures, examples being lane formation [1,2], shear banding [3], the coiling up of magnetic chains [4], and the wide range of patterns observed in particles immersed in liquid crystals [5]. Here, we are particularly interested in colloidal systems involving dipolar interactions. Prime examples of the resulting self-assembled structures include chain formation in constant external fields [6–8], layer formation in rotating fields [7–10], and the structure formation of colloidal particles in triaxial fields [11–13].

Until recently, most works on self-organization under the influence of time-dependent external fields focused on *induced* dipolar particles. A noteworthy exception is a paper by Murashov and Patey in which layer formation of rotationally driven colloidal particles carrying a permanent dipole moment was investigated [14].

A particularly interesting self-organization process occurs when colloidal particles are exposed to rotating fields in a quasi-two-dimensional geometry. In this situation, the external fields are found to induce the formation of two-dimensional clustered structures. Not only does this work for particles in which a dipole moment can be induced [15–17], but also for particles carrying a permanent dipole moment. This was recently shown by Weddemann and coworkers in an experimental study [18,19].

In the present paper, we want to pick up on this phenomenon and provide a novel interpretation of the two-dimensional cluster formation process. Specifically, we will show that this self-organization process is a consequence of an equilibrium phase transition between a vapor and a condensed phase.

We investigate the colloidal system by making use of different computer simulation techniques. In these simulations, we use dipolar particles in a quasi-two-dimensional geometry to model the system. This means that the dipoles can rotate freely in all the spatial directions while the translational motion is restricted to a two-dimensional plane. We use Langevin dynamics simulations to understand the dynamical properties of the system and Wang-Landau Monte Carlo simulations to look into its phase behavior. Additionally, to assess the influence of the solvent on the system, we take it implicitly into account by employing Brownian dynamics simulations that include hydrodynamic interactions.

This paper is organized as follows: After introducing the model and the different simulation techniques, we first discuss the full nonequilibrium "phase" diagram indicating the region of cluster formation in the domain of frequency and strength of the external field at constant equilibrium thermodynamic parameters. In a next step, we investigate the influence of hydrodynamic interactions on the formation of clusters. Then we present the principal point of this paper: We show that the nonequilibrium cluster formation is essentially an equilibrium phase transition. To do this, we calculate an equilibrium phase diagram, in the construction of which an effective non-time-dependent interparticle interaction is used, and examine the growth of the characteristic domain size of the clusters. The paper is then closed with a brief summary and conclusions.

II. MODEL AND SIMULATION METHODS

To model the (dipolar) colloidal particles in our simulations we use a dipolar soft sphere (DSS) potential, which is comprised of a repulsive part U^{rep} and a point dipole-dipole interaction part U^{D}:

$$U^{\mathrm{DSS}}(\mathbf{r}_{ij},\boldsymbol{\mu}_i,\boldsymbol{\mu}_j) = U^{\mathrm{rep}}(r_{ij}) + U^{\mathrm{D}}(\mathbf{r}_{ij},\boldsymbol{\mu}_i,\boldsymbol{\mu}_j). \qquad (1)$$

In Eq. (1), $\mathbf{r}_{ij}$ is the vector between the positions of the particles i and j, r_{ij} its absolute value, and $\boldsymbol{\mu}_i$ is the dipole moment of the ith particle. The dipolar and repulsive interaction potentials are given by

$$U^{\mathrm{D}}(\mathbf{r}_{ij},\boldsymbol{\mu}_i,\boldsymbol{\mu}_j) = -\frac{3(\mathbf{r}_{ij}\cdot\boldsymbol{\mu}_i)(\mathbf{r}_{ij}\cdot\boldsymbol{\mu}_j)}{r_{ij}^5} + \frac{\boldsymbol{\mu}_i\cdot\boldsymbol{\mu}_j}{r_{ij}^3} \qquad (2)$$

*jaeger@itp.tu-berlin.de

and

$$U^{\mathrm{rep}}(r) = U^{\mathrm{SS}}(r) - U^{\mathrm{SS}}(r_c) + (r_c - r)\frac{dU^{\mathrm{SS}}}{dr}(r_c), \quad (3)$$

respectively. Here, U^{rep} is the shifted soft sphere potential, where

$$U^{\mathrm{SS}}(r) = 4\epsilon\left(\frac{\sigma}{r_{ij}}\right)^{12} \quad (4)$$

is the unshifted soft sphere (SS) potential for particles of diameter σ.

Note that we use the DSS potential to model the dipolar particles instead of the frequently used Stockmayer potential (see, e.g., [20]). The latter has an additional short-ranged isotropic, attractive part, modeling the van der Waals interaction, which has a considerable influence on the phase behavior of the system. In particular, it can induce a vapor-liquid phase transition [21,22] that has so far not been found in dipolar systems lacking a spherically symmetric, attractive interaction [23]. Here we are interested in the effects of the dipolar interactions on the phase behavior alone, which is why we discard the short-ranged attractive part.

We investigate the system by making use of different simulation techniques. First, we employ Langevin dynamics (LD) simulations [14,24]. The corresponding equations of motion for particles of mass m and moment of inertia I are

$$m\ddot{\mathbf{r}}_i = \mathbf{F}_i^{\mathrm{DSS}} - \xi_T\dot{\mathbf{r}}_i + \mathbf{F}_i^{\mathrm{G}}, \quad (5)$$

$$I\dot{\boldsymbol{\omega}}_i = \mathbf{T}_i^{\mathrm{DSS}} + \mathbf{T}_i^{\mathrm{ext}} - \xi_R\boldsymbol{\omega}_i + \mathbf{T}_i^{\mathrm{G}}, \quad (6)$$

where ξ_T and ξ_R are the translational and rotational friction coefficients, respectively, and

$$\mathbf{F}_i^{\mathrm{DSS}} = -\boldsymbol{\nabla}U_i^{\mathrm{DSS}}, \quad (7)$$

$$\mathbf{T}_i^{\mathrm{DSS}} = -\boldsymbol{\mu}_i \times \boldsymbol{\nabla}_{\boldsymbol{\mu}_i}U_i^{\mathrm{DSS}}, \quad (8)$$

$$\mathbf{T}_i^{\mathrm{ext}} = \boldsymbol{\mu}_i \times \mathbf{B}. \quad (9)$$

Consistent with earlier simulation studies of ferrofluidic particles [10,14], $\xi_T = 13.5\sqrt{m\epsilon/\sigma^2}$, $\xi_R = 0.45\sqrt{m\epsilon\sigma^2}$, and $I = 0.0025m\sigma^2$ were used. Furthermore, $\boldsymbol{\omega}_i$ is the angular velocity of particle i, $\mathbf{F}_i^G$ and $\mathbf{T}_i^G$ are random Gaussian forces and torques with zero mean

$$\left\langle F_{i\alpha}^G(t)\right\rangle = 0, \quad (10)$$

$$\left\langle T_{i\beta}^G(t)\right\rangle = 0, \quad (11)$$

whose variance is related to the friction coefficients via

$$\left\langle F_{i\alpha}^G(t)F_{j\beta}^G(t')\right\rangle = 6k_BT\xi_T\delta_{ij}\delta_{\alpha\beta}\delta(t-t'), \quad (12)$$

$$\left\langle T_{i\alpha}^G(t)T_{j\beta}^G(t')\right\rangle = 6k_BT\xi_R\delta_{ij}\delta_{\alpha\beta}\delta(t-t') \quad (13)$$

($\alpha,\beta = x,y$) [14]. In Eq. (9), the external field $\mathbf{B}$ is homogeneous, rotates in the plane of the dipolar monolayer, and is given by

$$\mathbf{B}(t) = B_0(\mathbf{e}_x\cos\omega_0 t + \mathbf{e}_y\sin\omega_0 t), \quad (14)$$

where ω_0 is the frequency of the field and B_0 its strength. The equations of motion (5) and (6) were integrated with a leapfrog algorithm [25] using a time step of $\Delta t = 0.0025(m\sigma^2/\epsilon)^{1/2}$ and 4900 or 1225 particles, respectively.

Further, to investigate the influence of a solvent within our implicit model, we use a Brownian dynamics (BD) simulation that includes hydrodynamic interactions between the particles. These interactions are incorporated up to third order in the diffusion tensor for the translation-translation coupling, the rotation-rotation coupling, and the translation-rotation (and vice versa) coupling [26,27]. The tensor describing the translation-translation coupling is the well known Rotne-Prager tensor. The other couplings incorporate the influence of the additional rotational degrees of freedom. The time evolution equations that were used can be found in [27] and we used 324 particles in these simulations.

Finally, to investigate the equilibrium phase behavior of the system [based on a time-averaged potential, see Eq. (16)], we use Monte Carlo (MC) simulations in the grand canonical ensemble. In general, first-order phase transitions are plagued by a large free energy barrier separating both phases, making unbiased sampling very inefficient. In order to overcome the barrier we use an extension of a method proposed by Wang and Landau [28]. In the standard Wang-Landau method the entire density of states is sampled, which is infeasible in dipolar systems due to the computational cost. To account for this we fix the temperature and chemical potential in our simulations to limit the number of accessible states. Furthermore, we introduce an additional weight function to the Metropolis MC sampling algorithm. This function is computed on the fly and adapted in such a way that it improves the sampling of states which have not been visited sufficiently often. This allows us to sample both phases efficiently despite them being separated by a free energy barrier. Details of the method applied to dipolar systems in two dimensions can be found in [29].

In the case of LD and MC simulations we deal with the long-ranged dipolar interactions by using the Ewald summation method [30]. In our BD simulations (with and without hydrodynamic interactions included), on the other hand, we only consider a single simulation box filled with dipolar particles. This suffices to investigate the influence of the hydrodynamic interactions on the cluster formation.

III. RESULTS

In this section, we present numerical results from the various simulation techniques described in Sec. II. We begin with results from the Langevin dynamics simulations, the goal being to determine the conditions (i.e., frequencies, field strengths) for which cluster formation occurs. We also introduce the equilibrium model resulting from a time-average of the interactions in the driven system. In Sec. III B, we focus on the influence of hydrodynamic interactions in the field-driven system. Sections III C and III D are then devoted to the question of whether the clustering phenomenon is indeed related to a condensation transition of the equilibrium model. To this end we determine a phase coexistence curve [Sec. III C] and, as a final step, investigate the growth of domain sizes (within the two-phase region of the phase diagram) as function of time.

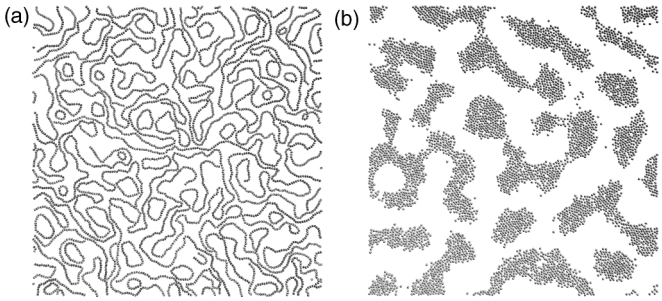

FIG. 1. Snapshots showing a system ($\rho\sigma^2 = 0.3$, $k_BT/\epsilon = 1.0$) in (a) zero field and (b) exposed to a rotating field of strength $(\epsilon/\sigma^3)^{1/2}B_0 = 50.0$ and frequency $(m\sigma^2/\epsilon)^{-1/2}\omega_0 = 20$. Snapshot (b) was taken at time $t = 375(m\sigma^2/\epsilon)^{1/2}$ after the start of the simulation. 4900 particles were used. Note that the configuration shown in (b) is not in equilibrium [cf. Sec. III C].

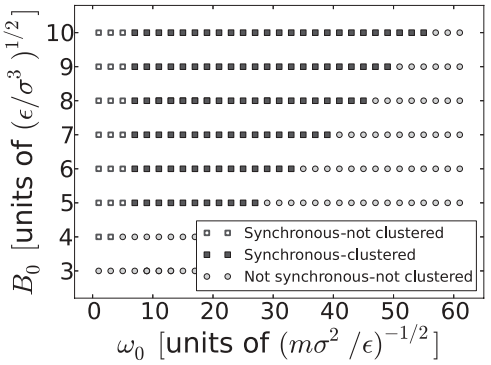

FIG. 2. Synchronization behavior and cluster formation depending on frequency ω_0 and strength B_0 of the field. The density and temperature of the system used were $\rho\sigma^2 = 0.2$ and $k_BT/\epsilon = 1.0$, respectively.

A. Synchronization and cluster formation

A snapshot of a quasi-two-dimensional system ($\rho\sigma^2 = 0.3$, $k_BT/\epsilon = 1.0$) of strongly coupled dipolar particles ($\lambda_{DD} = \mu^2/k_BT\sigma^3 = 9$) at zero field is shown in Fig. 1(a). As is typical for such dipolar systems the particles align in a head-to-tail configuration, which, in a two-dimensional geometry, results in the formation of chains and rings [31].

If we expose such a strongly coupled system to a rotating in-plane field of sufficient strength and frequency, we observe that the particles agglomerate into two-dimensional clusters. An example of this can be seen in Fig. 1(b). The observed clustering behavior already indicates that there are attractive interactions in the system, which play a crucial role. The origin of these interactions can be rationalized as follows: Assume that the particles do not move in space and that they rotate synchronously with the field, i.e., follow the field at constant phase difference δ:

$$\boldsymbol{\mu}_i(t) = \boldsymbol{\mu}_j(t) = \mu(\mathbf{e}_x \cos(\omega_0 t + \delta) + \mathbf{e}_y \sin(\omega_0 t + \delta)). \quad (15)$$

Averaging the dipolar interaction potential over one rotational period of the field then yields [32]

$$U^{\mathrm{ID}}(\mathbf{r}_{ij}) = \frac{\omega_0}{2\pi}\int_{t_0}^{t_0+2\pi/\omega_0} U^{\mathrm{D}}(\mathbf{r}_{ij},\boldsymbol{\mu}_i(t),\boldsymbol{\mu}_j(t))dt = -\frac{\mu^2}{2r_{ij}^3}. \quad (16)$$

Clearly, for (16) to be a good approximation to the true interparticle interaction, it is crucial that essentially all the particles follow the field. An extensive analysis of this synchronization behavior of the dipolar particles with the field in three dimensions can be found in [10,33].

To systematically investigate the appearance of synchronization and clustering we scanned a wide range of frequencies and field strengths in a system containing 1225 particles. We consider a system as clustered if the particles have on average more than 2.3 neighbors within a distance of 1.7σ from their center. The latter value was used, since it is slightly larger than the typical distance between neighboring particles in a clustered system at high frequencies of the field. This was found by looking at the first minimum of respective pair correlation functions. The fact that we require 2.3 neighbors on average ensures that two-dimensional aggregates are counted as clusters while chainlike structures are disregarded. Using larger values for the required number of neighbors results in a shift of the boundary between the synchronous region and the clustered region to higher frequencies. Responsible for this is the fact that the clusters become tighter with rising frequencies due to the effective interaction between the particles becoming more isotropic.

The results of this investigation of the space of the field parameters can be seen in Fig. 2. Depicted are three distinct regions, denoted "synchronous–not clustered," "synchronous-clustered," and "not synchronous–not clustered." The first region is comprised of systems in which the particles rotate synchronously with the field but do not form clusters. Within this region, chains in the direction of the field can be observed at low frequencies while spatial inhomogeneities, i.e., very loose clusters, begin to appear at slightly larger frequencies. As also becomes apparent here, a minimal B_0 is required for the field to align the particles with itself.

In the second region, the synchronous rotation continues but is now accompanied by the formation of two-dimensional clusters. This indicates that the effective interparticle potential becomes sufficiently isotropic within this region to be reasonably described by the averaged dipolar potential (16).

In the third region, we find neither synchronization nor cluster formation. Clearly, the lack of synchronization is the direct cause of the breakdown of cluster formation [cf. Eq. (16)]. The loss of synchronization occurs, since the torques on the particles due to the external field become unable to overcome the torques due to the rotational friction (similarly to what is seen in three dimensions [10]).

In a previous publication [10], we have presented a similar diagram for layer formation of rotationally driven dipolar particles in three dimensions. The mechanism leading to the formation of layers is quite similar to the one described here resulting in a ω_0-B_0 diagram that resembles the one depicted in Fig. 2. Synchronization breaks down at high frequencies close to a critical frequency $\omega_c(B_0)$ (cf. [10]), leading to the breakdown of layer formation and cluster formation. Also, the strength of the field needs to be sufficiently high to align the particles with itself. A difference can be found in the minimal driving frequency that is required for the respective pattern formation to occur: Layers in three dimensions appear

at smaller frequencies than clusters do in two dimensions. This implies that symmetry breaking perpendicular to the field is less dependent on the frequency of the field than within its plane.

B. Influence of hydrodynamic interactions

Given the clustering scenario and our explanations so far, it is important to ask to which extent the LD simulations can describe the dynamics of the real colloidal system. The latter includes, by definition, a solvent. The rotating external field, which constantly generates rotational motion of the particles, will create flow fields that can result in considerable motion of the particles. This might influence the cluster formation phenomenon due to the following reason: The averaged potential (16) is only valid as an approximation to the true interparticle interaction if the translational motion of the particles during one rotational period of the field is small.

Hence, in order to find out whether cluster formation persists when hydrodynamic interactions are present, we perform BD simulations that take these into account. However, to restrict the numerical effort, we consider here a system without periodic boundaries; i.e., the particles are confined to a single simulation box. The particles interact with the walls of the simulation box via a repulsive, soft wall potential [34]. The influence of the walls on the hydrodynamic interactions is neglected.

We considered a number of state points ($\rho\sigma^2 = 0.1, 0.2, 0.3$, $k_BT/\epsilon = 1.0, 1.8$ at $\omega_0\sigma^2/D_0 = 250$, $B_0(\sigma^3/\epsilon)^{1/2} = 80$) in our BD simulations with and without hydrodynamic interactions included. Note that the frequency was reduced with the diffusion constant D_0 in these simulations, which makes a comparison to the frequencies used in the LD simulations difficult. As usual, D_0 is given by $D_0 = k_BT/3\pi\eta\sigma$, where η is the viscosity of the solvent. Further a very high field strength was chosen to ensure synchronization of the particles with the field [see Fig. 2]. We found that cluster formation occurs both with and without hydrodynamic interactions at all the considered densities and temperatures, with a single cluster eventually forming in the simulation box. This can be seen in Fig. 3, where we show snapshots of the time evolution of a rotationally driven system. The snapshots in the top row show a system in which hydrodynamic interactions are not taken into account, while hydrodynamic interactions are present in the snapshots in the lower row with the systems being identical otherwise. In both cases, no periodic boundary conditions were used. Another important point that is illustrated by Fig. 3 is that the cluster formation process is considerably accelerated by the hydrodynamic interactions. At the intermediate time ($t' = tD_0/\sigma^2 = 10.8$), only a single cluster remains in the hydrodynamically interacting system [Fig. 3(e)], while it takes much longer for the not hydrodynamically interacting system to reach the same state [cf. Figs. 3(b) and 3(c)].

Accelerated cluster formation is a direct consequence of both the translation-translation and rotation-translation coupling. A particularly important role in this context is played by the translation-translation coupling. This can be inferred from selectively switching off the different hydrodynamic couplings. Further, note that if hydrodynamic interactions are present, the cluster rotates rapidly around its center, which is not the case if these interactions are absent. Here, the sole cause is the hydrodynamic rotation-translation coupling. Thus, we can conclude that the hydrodynamic interactions affect the (rotational) cluster motion but do not hinder the particles in the cluster formation process.

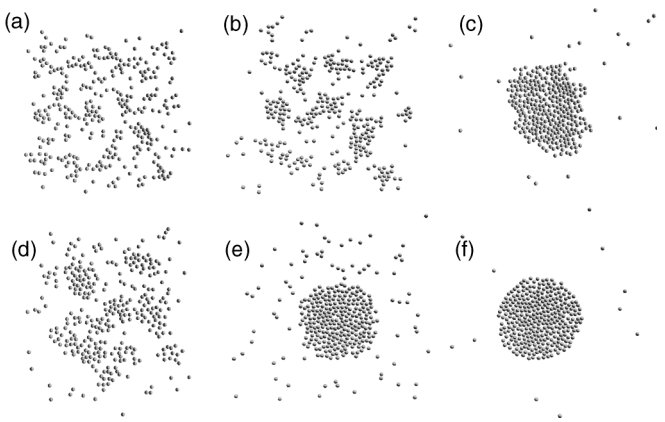

FIG. 3. Snapshots of a system ($(\epsilon\sigma^3)^{1/2}\mu = 3$, $k_BT/\epsilon = 1.0$, $\omega_0\sigma^2/D_0 = 200$, $B_0(\sigma^3/\epsilon)^{1/2} = 80$) at different times without (top) and with (bottom) hydrodynamic interactions. The snapshots in the first column were taken at $t' = tD_0/\sigma^2 = 2.5$ and the ones in the second column at $t' = 10.8$ after the start of the simulation. The ones in (c) and (f) correspond to the state of the system at $t' = 138.5$ and 43, respectively. These simulations do not include periodic boundary conditions. Instead, the particles are confined to a simulation box that is very large compared to the space that the particles are initially put into, ensuring minimal particle-wall interactions. Consequently, the snapshots do not show the entire simulation box but are centered on the clusters.

C. Relation to condensation

Now we ask to what extent the clustering behavior of the nonequilibrium, yet fully synchronized, field-driven system can be understood by that of a system interacting via Eq. (16), i.e., the effective potential U^{ID}. At sufficiently high strengths and frequencies of the field, this potential can be expected to describe the interaction between the particles very well without including an explicit time dependence. This allows us to test the following hypothesis: The observed cluster formation in the driven system stems from an equilibrium, first-order phase transition between a vapor and a condensed phase that arises due to the effective interparticle interaction U^{ID}. To this end, we perform Wang-Landau Monte Carlo simulations of a system interacting via the effective potential U^{ID} [35] combined with the repulsive potential U^{rep} [see Eq. (3)].

The key result we obtained from these simulations is the phase diagram presented in Fig. 4. The presence of the binodal in the phase diagram confirms our hypothesis: The nondriven system does indeed have an equilibrium phase transition between a vapor and a condensed phase.

Now we compare this phase diagram with the thermodynamic state point of the driven nonequilibrium system that is shown in Fig. 1(b). We find that the latter cannot be directly placed into Fig. 4, since its temperature is smaller than the ones displayed. However, the temperature of the state point ($\rho\sigma^2 = 0.3$, $k_BT/\epsilon = 1$) is considerably smaller than

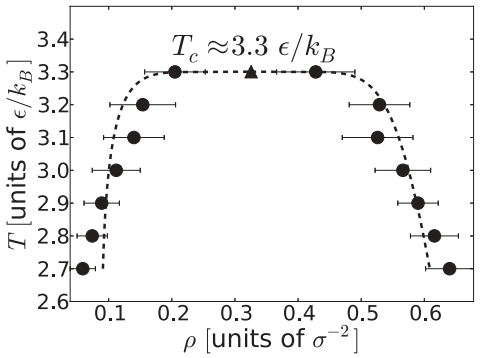

FIG. 4. Phase diagram in the T-ρ domain of a system interacting via the effective potential U^{ID} [see Eq. (16)] and the repulsive potential U^{rep} [see Eq. (3)] at $(\epsilon\sigma^3)^{1/2}\mu = 3$. The symbol T_c (indicated by the triangular mark) denotes the critical temperature, the dots correspond to the most often sampled densities, and the error bars to the width of the sampled distributions (cf. Ref. [29] for details). The solid line corresponds to the binodal representing coexisting gas and liquid states.

the critical temperature T_c, while its density is very close to the one of the critical point. This implies that the state lies well within the two-phase region of the phase diagram. Note that there are very few particles in between the clusters in Fig. 1(b). However, this is simply due to the temperature being low in relation to the critical temperature T_c. These findings suggest that the cluster formation observed in the (fully synchronized) field-driven system is in fact spinodal decomposition. We will come back to this point in Sec. III D.

Given our equilibrium binodal in Fig. 4, it is interesting to briefly compare our results with corresponding ones from a recent MC study of Smallenburg and Dijkstra [36]. These authors calculated full phase diagrams of systems of particles interacting via the effective potential U^{ID} in three dimensions. Consistent with our findings in two dimensions, the authors found a vapor-liquid coexistence region.

Additionally, Smallenburg and Dijkstra uncovered an adjacent vapor-solid coexistence region [36]. We suspect that a corresponding region also exists in our two-dimensional system, although this is not easily shown without free energy calculations. We also suspect that the type of coexistence (vapor-liquid or vapor-solid) would influence the structure of the clusters within the two-phase region. To investigate this, we performed test simulations of systems (interacting via U^{ID}) at several state points within the binodal of the phase diagram [Fig. 4]. Two exemplary snapshots are given in Fig. 5. Visual inspection suggests a solid-like (hexagonal) order at a temperature of $k_BT/\epsilon = 0.7$ [Fig. 5(a)], but not at $k_BT/\epsilon = 1.5$ [Fig. 5(b)]. To measure the degree of order quantitatively, we have calculated the hexagonal bond order parameter

$$\psi_6 = \frac{1}{N}\sum_{n=1}^{N}\frac{1}{|\mathcal{N}_n|}\left|\sum_{k\in\mathcal{N}_n}\exp(i6\pi\phi_{nk})\right| \qquad (17)$$

for these two systems. For the one at $k_BT/\epsilon = 0.7$, we found $\psi_6 \approx 0.78$, which is substantially higher than $\psi_6 \approx 0.53$, which we found for the $k_BT/\epsilon = 1.5$ system. In Eq. (17),

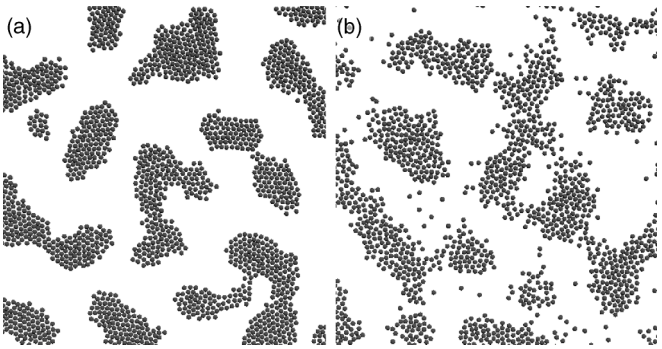

FIG. 5. Snapshots of (parts of) systems interacting via the effective potential U^{ID} at two different temperatures and density $\rho\sigma^2 = 0.3$. The temperature of the system depicted in (a) is $k_BT/\epsilon = 0.7$, the one of the system in (b) $k_BT/\epsilon = 1.5$. The snapshots were taken at time $t = 262.5(m\sigma^2/\epsilon)^{1/2}$ after the start of the simulation.

N is the number of particles in the simulation box, $\mathcal{N}_n$ is the set of neighbors of particle n, and ϕ_{nk} is the angle between a fixed but arbitrary axis and $\mathbf{r}_{nk}$. Further, two particles are considered neighbors if r_{nk} is smaller than the distance at which the first minimum of the pair correlation function is located. The relative difference in hexagonal order between the two systems indicates that the one at $k_BT/\epsilon = 0.7$ is indeed inside a vapor-solid coexistence region, while the lack of order in the $k_BT/\epsilon = 1.5$ system points to it still being within the vapor-liquid coexistence region. The temperature $k_BT/\epsilon = 1.0$ discussed before [Figs. 1 and 2] lies somewhere in between. However, more precise statements on the location of the triple point (or the very existence of a stable liquid phase) are impossible at this point.

D. Dynamic coarsening

We now come back to our conjecture in Sec. III C that the clustering process observed in the driven system corresponds to spinodal decomposition. To test this hypothesis, we investigated the time evolution of the cluster sizes ℓ. For phase separating systems it is well established that ℓ exhibits power law behavior [37], i.e., $\ell \propto t^{\alpha}$, with the corresponding exponents depending on the growth stage. Such a behavior is also seen in molecular dynamics (MD) simulations. In particular, domains with growth proportional to $t^{1/2}$ [38,39] and t [40] have been identified.

These power laws are universal in MD simulations but they do not necessarily apply to LD simulations with their modified equations of motion. This was shown, e.g., by Lodge and Heyes for the case of BD [41]. At the same time, however, the clusters in Ref. [41] were still found to grow with a power law. To check for the existence of cluster growth with a power law in non-overdamped BD simulations, i.e., LD simulations, we first investigated a "reference system" whose equilibrium behavior is well studied. Specifically, we considered a two-dimensional Lennard-Jones system at $\sigma^2 = 0.3$, $k_BT/\epsilon = 0.45$ with the critical point being at $\rho\sigma^2 \approx 0.335$, $k_BT/\epsilon \approx 0.533$ [42]. Investigating the domain size, we did indeed find a power law dependence $\ell \propto t^{\alpha}$ with $\alpha \approx 0.30$. Note that the cluster size was obtained by measuring the distance at which the pair correlation function assumes a value of one for the first time if

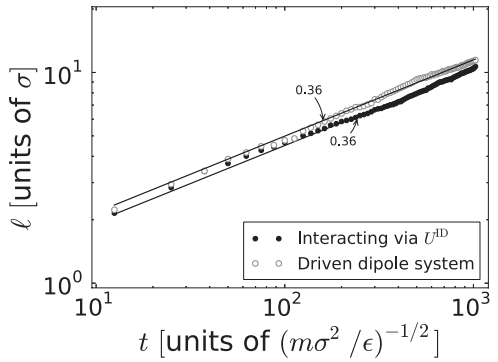

FIG. 6. Cluster growths for a system interacting via the effective potential and a system that is driven by an external rotating field at density $\rho\sigma^2 = 0.3$ and temperature $k_BT/\epsilon = 1.5$ (state inside the coexistence region of Fig. 4). The strength and frequency of the external field are $(\epsilon/\sigma^3)^{1/2}B_0 = 50$ and $(m\sigma^2/\epsilon)^{-1/2}\omega_0 = 20$, respectively.

the radial bins are taken to be larger than the particle diameters (cf. Ref. [43]).

Similarly, we checked the cluster growth for a driven dipolar system and a system interacting via the potential U^{ID}. In the simulations we used 4900 particles and a density and temperature of $\rho\sigma^2 = 0.3$ and $k_BT/\epsilon = 1.5$, respectively, which put the systems well inside the coexistence region of Fig. 4. The domain sizes over time that were extracted from the simulations are shown in Fig. 6. As can be seen, the cluster sizes of these two systems are very similar at any given time (on average the values deviate about 10% from each other). In particular, the characteristic domain sizes grow with a power law $\ell \propto t^{\alpha}$ with α being equal to 0.36 in both cases. We note that this is almost identical to the Lifshitz-Slyozov growth law ($\ell \propto t^{1/3}$) [37].

From these two results we conclude that the nonequilibrium system does indeed undergo spinodal decomposition. First, the cluster growth proceeds with a power law, which is typical within the spinodal region. Second, the growth behavior remains unchanged even if the interactions between the driven dipoles are replaced with the effective ones. This emphasizes the similarity between those two systems and indicates that the phase diagram for the effective system in Fig. 4 remains significant for the driven and synchronized system.

Note that hydrodynamic results are not included in Fig. 6. As pointed out in Sec. III B, we did not use periodic boundary conditions in these simulations. This makes an accurate determination of the cluster growth in the presence of hydrodynamic interactions very difficult.

IV. SUMMARY AND DISCUSSION

In this paper we have investigated the formation of two-dimensional aggregates in monolayers of dipolar particles that are driven by rotating external in-plane fields. The first result of this paper is a nonequilibrium "phase" diagram, which shows the regions of synchronization and cluster formation in the ω-B_0 domain. At high frequencies the synchronization of the particles with the field breaks down, which results in a breakdown of cluster formation. Similarly, we do not find cluster formation at low frequencies. Here, the effective interaction between the particles is not well enough described by U^{ID}, since the particles move considerably during one rotational period of the field. This changes in between those frequencies, where the particles rotate synchronously and sufficiently fast, which leads to the formation of clusters.

Next, we investigated the stability of the clustering phenomenon when hydrodynamic interactions are present. In our simulations, we found the phenomenon to persist despite these interactions. In fact, the cluster formation seems to proceed at an even faster pace with these interactions included. We attribute this to a combination of the hydrodynamic translation-translation and rotation-translation coupling. The former seems to accelerate the formation of clusters while the latter leads to the quick formation of a single cluster in the center of the simulation box.

Test simulations indicate that these interactions have additional consequences: Compared to a nonhydrodynamically interacting system, they seem to allow for the formation of clusters at lower driving frequencies and therefore affect the nonequilibrium "phase" diagram in Fig. 2. To study the precise influence of the hydrodynamic interactions is outside of the scope of this paper, but would be very illuminating in its own right.

We concluded our analysis with the main result of this study: We established the clustering phenomenon to be a consequence of a phase transition between a vapor and a condensed phase. This was done in two steps: We began by uncovering a phase transition via Wang-Landau MC simulations in a system interacting via the effective potential U^{ID}. Recall that this potential describes the interactions between the particles very well in the driven system at sufficiently high frequencies of the field. In a next step we examined the domain growth of the driven system within the binodal region of the phase diagram. As expected for spinodal decomposition, we found the characteristic cluster size to grow with a power law. Additionally, it essentially agrees with the domain growth of the nondriven system interacting via the effective potential U^{ID}. These facts lead us to conclude that the clustering process corresponds to the pattern formation occurring inside the coexistence region of a vapor-liquid phase transition.

Given these findings, it is interesting to compare them to recent experimental results. Indeed, cluster formation in monolayers resulting from a rotating external field has been observed multiple times [15–19]. In most of these publications induced dipolar particles are brought to self-assemble into two-dimensional aggregates. The only paper in which particles with a permanent dipole moment were used (Ref. [18]) features a dipole-dipole coupling strength ($\lambda_{\mathrm{DD}} = \mu^2/k_BT\sigma^3$) that is dominated by the dipole-field coupling strength ($\lambda_{\mathrm{DF}} = \mu B_0/k_BT$). There, the ratio $\lambda_{\mathrm{DF}}/\lambda_{\mathrm{DD}}$ is about 6, which is larger than the largest ratio that appears in Fig. 2. Consequently, we expect the particles in [18] to rotate synchronously with the field, resulting in the effective interaction U^{ID} and the observed cluster formation.

The clusters found in the literature are typically hexagonally ordered. In our simulations this becomes more and more true with increasing frequency and strength of the field as well as with decreasing temperature. The main reason for the difference between simulations and experiment is likely the difference in particle size: Micrometer-sized particles were

used in Refs. [15,17–19], resulting in large dipole-dipole coupling strengths λ_{DD}. This reduces the significance of the thermal motion compared to particles of smaller size, which usually have smaller coupling strengths. Indeed, at low temperatures, considerable hexagonal order [cf. Fig. 5] can be observed in our simulations. To have a full phase diagram of the effective system would be very helpful in this context: It would allow for a precise determination of the onset of hexagonal order in the system and the general structural order of the colloidal suspension at any given state point (cf., e.g., Ref. [36] for details on how to determine the phase diagram via free energy calculations). This will be the subject of a future study.

Further, the driving frequencies used in the publications [15,17–19] are considerably smaller than the ones used here. This can once again be explained by the size of the particles: Larger particles typically have larger friction coefficients, which, as test simulations show, result in cluster formation at lower frequencies of the field. In fact, if we assume the particles to be about 1 μm in diameter with a density of 5 g/cm^3, we find a driving frequency of $\omega_0^* = 10$ to correspond to a frequency of about 10 kHz at room temperature ($T = 293$ K).

In this paper, we used specific friction coefficients in our Langevin simulations ($\xi_T = 13.5\sqrt{m\epsilon/\sigma^2}$, $\xi_R = 0.45\sqrt{m\epsilon\sigma^2}$). As suggested in the previous paragraph, the occurrence of cluster formation is, however, not exclusive to those. Indeed, in test simulations we found clusters at a multitude of different friction coefficients (e.g., at $\xi_T = 13.5\sqrt{m\epsilon/\sigma^2}$, $\xi_R\sqrt{1/m\epsilon\sigma^2} = 0.1,0.45,1,5$ and $\xi_R = 0.45\sqrt{m\epsilon\sigma^2}$, $\xi_T\sqrt{\sigma^2/m\epsilon} = 5,13.5,20,50,67.5$). These simulations indicate that the larger the translational friction coefficient, the smaller the frequency at which clusters begin to form. Increasing the rotational friction coefficient, on the other hand, seems to shift the breakdown of layer formation to lower frequencies of the field.

The coarsening process investigated in this paper can universally be observed in phase separating systems. Condensation transitions and spinodal demixing in binary fluids or metallic alloys are popular examples of this. The process reported in this study is exceptional, however, in that the existence of a liquid-vapor phase transition in ordinary dipolar soft and hard sphere systems without additional (van der Waals like) attraction is still a hotly debated topic and one of the big unresolved questions regarding these particles [23,44,45]. But as shown here, such a phase transition can be induced via an external time-dependent field.

The system considered in this study is driven and, consequently, inherently in a nonequilibrium state. The dynamic coarsening observed in spinodal decomposition, on the other hand, is a process typically associated with nondriven systems. It is, however, not unique to those. Two examples are active Brownian swimmers performing a "run-and-tumble" motion such as E. coli bacteria [46] and self-propelled rods [47], both of which exhibit clustering behavior. With the ongoing and rising interest in dynamics and nonequilibrium processes we expect an increasing amount of systems to be uncovered that are driven into cluster or pattern formation with behaviors similar to the one described here.

ACKNOWLEDGMENTS

We gratefully acknowledge financial support from the DFG within the RTG 1558 *Nonequilibrium Collective Dynamics in Condensed Matter and Biological Systems* and IRTG 1524 *Self-Assembled Soft-Matter Nano-Structures at Interfaces*.

[1] J. Dzubiella, G. P. Hoffmann, and H. Löwen, Phys. Rev. E **65**, 021402 (2002).
[2] H. Löwen, Soft Matter **6**, 3133 (2010).
[3] K. Kang, M. P. Lettinga, Z. Dogic, and J. K. G. Dhont, Phys. Rev. E **74**, 026307 (2006).
[4] N. Casic, S. Schreiber, P. Tierno, W. Zimmermann, and T. M. Fischer, Europhys. Lett. **90**, 58001 (2010).
[5] U. Ognysta, A. Nych, V. Nazarenkom, M. Škarabot, and I. Muševič, Langmuir **25**, 12092 (2009).
[6] J. E. Martin, R. A. Anderson, and C. P. Tigges, J. Chem. Phys. **108**, 3765 (1998).
[7] J. E. Martin, R. A. Anderson, and C. P. Tigges, J. Chem. Phys. **110**, 4854 (1999).
[8] J. E. Martin, E. Venturini, J. Odinek, and R. A. Anderson, Phys. Rev. E **61**, 2818 (2000).
[9] M. E. Leunissen, H. R. Vutukuri, and A. v. Blaaderen, Adv. Mater. **21**, 3116 (2009).
[10] S. Jäger and S. H. L. Klapp, Soft Matter **7**, 6606 (2011).
[11] J. E. Martin, E. Venturini, G. L. Gulley, and J. Williamson, Phys. Rev. E **69**, 021508 (2004).
[12] N. Osterman, I. Poberaj, J. Dobnikar, D. Frenkel, P. Ziherl, and D. Babić, Phys. Rev. Lett. **103**, 228301 (2009).
[13] J. F. Douglas, Nature (London) **463**, 302 (2010).
[14] V. V. Murashov and G. N. Patey, J. Chem. Phys. **112**, 9828 (2000).
[15] N. Elsner, C. P. Royall, B. Vincent, and D. R. E. Snoswell, J. Chem. Phys. **130**, 154901 (2009).
[16] P. Tierno, R. Muruganathan, and T. M. Fischer, Phys. Rev. Lett. **98**, 028301 (2007).
[17] D. R. E. Snoswell, C. L. Bower, P. Ivanov, M. J. Cryan, J. G. Rarity, and B. Vincent, New J. Phys. **8**, 267 (2006).
[18] A. Weddemann, F. Wittbracht, B. Eickenberg, and A. Hütten, Langmuir **26**, 19225 (2010).
[19] F. Wittbracht, B. Eickenberg, A. Weddemann, and A. Hütten, in *ICQNM 2011, The Fifth International Conference on Quantum, Nano and Micro Technologies*, edited by V. Privman (Curran Associates, Inc., 2012), p. 99.
[20] M. J. Stevens and G. S. Grest, Phys. Rev. E **51**, 5976 (1995).
[21] M. E. van Leeuwen and B. Smit, Phys. Rev. Lett. **71**, 3991 (1993).
[22] B. Groh and S. Dietrich, Phys. Rev. E **50**, 3814 (1994).
[23] L. Rovigatti, J. Russo, and F. Sciortino, Phys. Rev. Lett. **107**, 237801 (2011).
[24] Z. Wang, C. Holm, and H. W. Müller, Phys. Rev. E **66**, 021405 (2002).

[25] M. P. Allen and D. J. Tildesley, *Computer Simulations of Liquids* (Oxford University Press, 1986).
[26] E. Dickinson, S. A. Allison, and J. A. McCammon, J. Chem. Soc., Faraday Trans. 2 **81**, 591 (1985).
[27] G. Mériguet, M. Jardat, and P. Turq, J. Chem. Phys. **123**, 144915 (2005).
[28] F. Wang and D. P. Landau, Phys. Rev. Lett. **86**, 2050 (2001).
[29] H. Schmidle and S. H. L. Klapp, J. Chem. Phys. **134**, 114903 (2011).
[30] J. J. Weis, J. Phys.: Condens. Matter **15**, 1471 (2003).
[31] P. D. Duncan and P. J. Camp, J. Chem. Phys. **121**, 11322 (2004).
[32] T. C. Halsey, R. A. Anderson, and J. E. Martin, Int. J. Mod. Phys. B **10**, 3019 (1996).
[33] S. Jäger and S. H. L. Klapp, Magnetohydrodynamics **47**, 135 (2011).
[34] S. Grandner and S. H. L. Klapp, J. Chem. Phys. **129**, 244703 (2008).
[35] We calculated the energy contribution of (16) via the well known dipolar Ewald sum. This can be done, since the dipole-dipole energy essentially reduces to U^{ID}, if the dipoles are oriented perpendicular to the monolayer (cf. [36]).
[36] F. Smallenburg and M. Dijkstra, J. Chem. Phys. **132**, 204508 (2010).
[37] R. C. Desai and R. Kapral, *Dynamics of Self-Organized and Self-Assembled Structures* (Cambridge University Press, 2009).
[38] S. W. Koch, R. C. Desai, and F. F. Abraham, Phys. Rev. A **27**, 2152 (1983).
[39] H. Kabrede and R. Hentschke, Physica A **361**, 485 (2006).
[40] S. Majumder and S. K. Das, Europhys. Lett. **95**, 46002 (2011).
[41] J. F. M. Lodge and D. M. Heyes, J. Chem. Soc., Faraday Trans. **93**, 437 (1997).
[42] J. A. Barker, D. Henderson, and F. F. Abraham, Physica A **106**, 226 (1981).
[43] F. F. Abraham, S. W. Koch, and R. C. Desai, Phys. Rev. Lett. **49**, 923 (1982).
[44] G. Ganzenmüller, G. N. Patey, and P. C. Campa, Mol. Phys. **107**, 403 (2009).
[45] J. Russo, J. M. Tavares, P. I. C. Teixeira, M. M. Telo da Gama, and F. Sciortino, Phys. Rev. Lett. **106**, 085703 (2011).
[46] J. Tailleur and M. E. Cates, Phys. Rev. Lett. **100**, 218103 (2008).
[47] F. Ginelli, F. Peruani, M. Bär, and H. Chaté, Phys. Rev. Lett. **104**, 184502 (2010).